

# Near collapse of the meridional SST gradient in the eastern equatorial Pacific during Heinrich Stadial 1

Stephanie S. Kienast,<sup>1</sup> Tobias Friedrich,<sup>2</sup> Nathalie Dubois,<sup>3</sup> Paul S. Hill,<sup>1</sup>  
Axel Timmermann,<sup>2</sup> Alan C. Mix,<sup>4</sup> and Markus Kienast<sup>1</sup>

Received 20 April 2013; revised 30 July 2013; accepted 3 October 2013; published 25 November 2013.

[1] Sea surface temperatures (SST) and inorganic continental input over the last 25,000 years (25 ka) are reconstructed in the far eastern equatorial Pacific (EEP) based on three cores stretching from the equatorial front ( $\sim 0.01^\circ\text{N}$ , ME0005-24JC) into the cold tongue region ( $\sim 3.6^\circ\text{S}$ ; TR163-31P and V19-30). We revisit previously published alkenone-derived SST records for these sites and present a revised chronology for V19-30. Inorganic continental input is quantified at all three sites based on  $^{230}\text{Th}$ -normalized fluxes of the long-lived continental isotope thorium-232 and interpreted to be largely dust. Our data show a very weak meridional (cross-equatorial) SST gradient during Heinrich Stadial 1 (HS1, 18–15 ka B.P.) and high dust input along with peak export production at and north of the equator. These findings are corroborated by an Earth system model experiment for HS1 that simulates intensified northeasterly trade winds in the EEP, stronger equatorial upwelling, and surface cooling. Furthermore, the related southward shift of the Intertropical Convergence Zone (ITCZ) during HS1 is also indicative of drier conditions in the typical source regions for dust.

**Citation:** Kienast, S. S., T. Friedrich, N. Dubois, P. S. Hill, A. Timmermann, A. C. Mix, and M. Kienast (2013), Near collapse of the meridional SST gradient in the eastern equatorial Pacific during Heinrich Stadial 1, *Paleoceanography*, 28, 663–674, doi:10.1002/2013PA002499.

## 1. Introduction

[2] The ocean and atmosphere are tightly coupled in the eastern equatorial Pacific (EEP) by the presence of a shallow and steep thermocline [Mitchell and Wallace, 1992], allowing this region to undergo large sea surface temperature (SST) changes on short timescales. On interannual timescales, SST perturbations in the EEP, which are related to the El Niño–Southern Oscillation (ENSO), drive changes in the large-scale Walker circulation and trigger stationary atmospheric waves which can affect climate in remote areas [Schneider et al., 2012; Joly and Voldoire, 2009; Sakai and Kawamura, 2009, and references therein]. Changes in ENSO amplitude have been linked to changes in the EEP annual cycle strength, which in turn is controlled by the strong meridional SST gradient between the Eastern Pacific Warm Pool (EPWP,  $>27.5^\circ\text{C}$ ), located north of the equator, and the cold tongue region, centered around  $1^\circ$  south of the

equator (Figure 1) [e.g., Timmermann et al., 2007a]. The EEP also plays an important role for global biogeochemical cycles. On annual to decadal timescales, it is the single largest oceanic source of  $\text{CO}_2$  to the atmosphere [Takahashi et al., 2009]. Despite being a high-nutrient, low-chlorophyll region, where phytoplankton are colimited by iron (Fe) and silicic acid (Si) [e.g., Coale et al., 1996; Brzezinski et al., 2011; Dugdale et al., 2011], the EEP hosts 18–56% of global oceanic export production [Chavez and Barber, 1987].

[3] The paleoceanographic interpretation of EEP sedimentary records, in particular for the last 25 ka, has been complicated by the fact that different SST proxies yield conflicting results with respect to the spatial distribution and timing of deglacial changes in SSTs [Lea et al., 2006; Koutavas and Sachs, 2008; Dubois et al., 2009]. In addition, lateral sediment redistribution along the seafloor can severely bias age-model-based estimates of past particle rain from the sea surface to the seafloor [e.g., Marcantonio et al., 2001; Kienast et al., 2007; Singh et al., 2011].

[4] The objective of this study is twofold. First, using three sediment cores from the EEP (Figure 1 and Table 1), we quantify the meridional SST gradient in the far eastern EEP over the last 25 ka in order to contribute to a better understanding of the ocean–atmosphere system in EEP and its connection to the North Atlantic during Heinrich Stadial 1 (HS1). Second, we reconstruct inorganic continental input to the EEP in order to examine whether a previously recognized maximum in export production in this region is related to fertilization by dust input. In order to complement our physical understanding of wind and upwelling changes in

<sup>1</sup>Department of Oceanography, Dalhousie University, Halifax, Nova Scotia, Canada.

<sup>2</sup>International Pacific Research Center, SOEST, University of Hawaii, Honolulu, Hawaii, USA.

<sup>3</sup>Woods Hole Oceanographic Institution, Woods Hole, Massachusetts, USA.

<sup>4</sup>College of Earth, Ocean and Atmospheric Sciences, Oregon State University, Corvallis, Oregon, USA.

Corresponding author: S. S. Kienast, Department of Oceanography, Dalhousie University, 1355 Oxford Street PO Box 15000, Halifax, NS B3H 4R2, Canada. (stephanie.kienast@dal.ca)

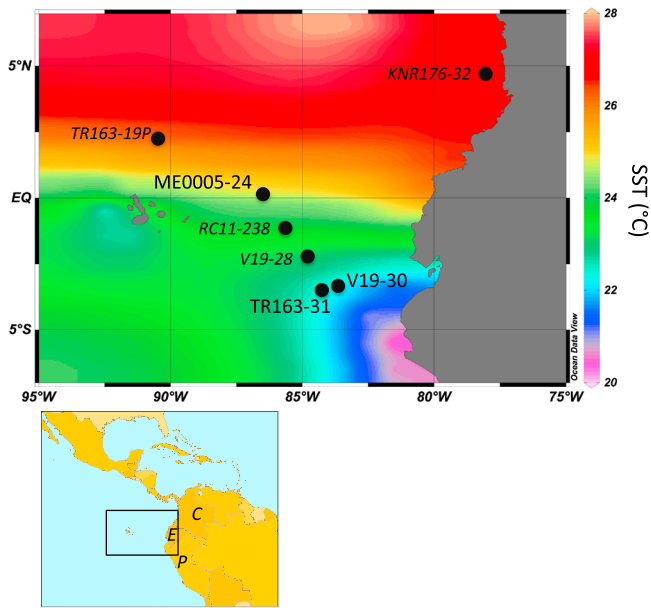


**Figure 1.** Core locations in the eastern equatorial Pacific plotted on mean annual SST distributions [Locarnini *et al.*, 2010]. Sites ME0005-24JC, TR163-31P, and V19-30 are the focus of this study; additional sites are plotted for reference. C: Colombia; E: Ecuador, P: Peru.

this complex region, we simulate a weakening of the Atlantic meridional overturning circulation (AMOC) during HS1 with the LOVECLIM 1.2 Earth system model of intermediate complexity [Goosse *et al.*, 2010].

## 2. Study Area

[5] A strong meridional SST gradient exists between the EPWP and the equatorial cold tongue region (Figure 1). The EPWP is the result of a seasonally large heat flux and weak wind mixing [Wang and Enfield, 2001; Fiedler and Talley, 2006]. Lower SSTs in the cold tongue region are maintained by upwelling-favorable southeasterly trade winds, which blow year-round across the equator into the Intertropical Convergence Zone (ITCZ). Over the course of the year, SSTs in the cold tongue are lowest and southeasterly trade winds strongest in late boreal summer (September), 3 months after the ITCZ reached its northernmost (14°N) position in June. During the warm phase of ENSO (El Niño), the cold tongue weakens in the EEP, and the meridional and zonal SST gradients collapse. The meridional asymmetry of surface climatology across the equator is a key factor in determining tropical eastern Pacific mean climate, annual cycle, and variability. In close connection to the seasonal migration of the ITCZ, the meridional SST gradient in the EEP drives

cross-equatorial winds and essentially sets up the annual cycle in the EEP [Xie, 1994; Timmermann *et al.*, 2007a]. The strength of the annual cycle in the EEP is thought to covary with the AMOC [Timmermann *et al.*, 2007b].

[6] Interpolating from a limited number of globally distributed field observations, Duce *et al.* [1991] estimate that under present-day conditions  $0.1\text{--}1\text{ g m}^{-2}\text{ yr}^{-1}$  of mineral aerosols (dust) are deposited in the EEP. Modeling studies give comparable estimates of  $0.2\text{--}0.5\text{ g m}^{-2}\text{ yr}^{-1}$  [Jickells *et al.*, 2005; Mahowald *et al.*, 2006]. This makes the EEP a relatively dust-starved region in comparison with the eastern equatorial Atlantic for example, where dust deposition rates are at least an order of magnitude higher [Jickells *et al.*, 2005; Mahowald *et al.*, 2006] due to the relative proximity to the Sahara. Mahowald [2007] included a source apportionment in their model and found that the equatorial North Pacific receives dust mainly from African sources. Prospero and Bonatti [1969] sampled atmospheric dust in the EEP directly using nylon mesh panels and observed two distinct mineralogical compositions north and south of the equator. However, rather than Africa, they suggest that the arid regions in western and southern Mexico act as principal dust sources to the northern EEP. The low-pressure region of the ITCZ is thought to act as an effective barrier to mixing of air masses [e.g., Stehr *et al.*, 2002] and dust transport [Rea, 1994; Prospero and Bonatti, 1969] between the Northern and Southern Hemispheres. Under present-day conditions, the ITCZ migrates from  $\sim 5^\circ\text{N}$  in January to  $14^\circ\text{N}$  in June and remains to the north of our sites year-round.

## 3. Approach of This Study

[7] In order to reconstruct the meridional SST gradient in the EEP, we revisit previously published SST reconstructions from three cores (Figure 1 and Table 1). Site ME0005-24JC is located close to the southern boundary of the EPWP in the equatorial front. The more southerly sites V19-30 and TR163-31P are situated in the cold tongue region. Note that a revised chronology is presented for site V19-30 (see section 4.7. below).

[8] As a tracer for continental material, we use  $^{232}\text{Th}$ , also known as primordial thorium because of its long half-life ( $1.4 \times 10^{10}$  years). Thorium-232 concentrations in continental dust ( $\sim 10.7$  ppm) are almost an order of magnitude greater than those in mid-ocean ridge basalt-like material ( $\sim 0.2$  ppm) and do not vary significantly between source regions [McGee *et al.*, 2007; Taylor and McClennan, 1985]. Winckler *et al.* [2008] measured  $^{230}\text{Th}$ -normalized fluxes of  $^{232}\text{Th}$  in cores from the equatorial Pacific west of  $110^\circ\text{W}$  and inferred elevated dust fluxes during glacial periods over the last 400 kyr, synchronous with enhanced dust fluxes reconstructed from Antarctic ice cores. We follow the approach of this earlier study with the goal of delineating the history of dust deposition in the far eastern EEP. Our core sites ( $83\text{--}86^\circ\text{W}$ ) are located much

**Table 1.** Cores Used in This Study<sup>a</sup>

	Water Depth (m)	Longitude	Latitude	Mean Annual SST (°C)	Distance to Coast (km)
ME0005-24JC	2941	86°27.788' W	0°01.302'N	24.8	~600
V19-30	3091	83°31'W	3°23'S	21.7	~275
TR163-31P	3209	83°57'W	3°35'S	21.8	~330

<sup>a</sup>Mean annual SST data taken from the World Ocean Atlas 2009 [Locarnini *et al.*, 2010]. Distance to coast is estimated by multiplying the difference in longitude at the core sites and the coastline by 111 km.

further east than the easternmost site of *Winckler et al.* [2008] and offer higher sedimentation rates and thus higher temporal resolution through the last deglaciation.

[9] Following *Winckler et al.* [2008], we quantify  $^{232}\text{Th}$  flux by normalizing  $^{232}\text{Th}$  concentrations to  $^{230}\text{Th}$  [*Bacon*, 1984; *Francois et al.*, 2004, and references therein]. Normalization of sedimentary components to the activity of the particle-reactive isotope  $^{230}\text{Th}$  has been proposed as a means to more accurately determine vertical particle fluxes originating from the sea surface compared to the traditional age-model-based mass accumulation rate (MAR) approach. Indeed, Th-normalized fluxes of organic carbon display a coherent regional pattern during the Holocene in the EEP that is consistent with modern primary production [*Kienast et al.*, 2007]. Two nearby sites in the EEP, which are less than 10 km apart, show nearly identical bulk fluxes over the last 30 ka when normalized to  $^{230}\text{Th}$ , which is not the case for MARs derived for the same sites [*Kienast et al.*, 2007]. However, Th normalization remains contested in the EEP, because Th-normalized fluxes are often much higher than MAR values, implying a significant role for sediment redistribution (i.e., focusing) [e.g., *Marcantonio et al.*, 2001; *Loubere et al.*, 2004; *Paytan et al.*, 2004; *Francois et al.*, 2004, 2007; *Loubere and Richaud*, 2007; *Lyle et al.*, 2005, 2007; *Kienast et al.*, 2007; *Broecker*, 2008; *Siddall et al.*, 2008; *Singh et al.*, 2011, 2013; *Dubois and Mitchell*, 2012; *Mitchell and Huthnance*, 2013]. Sediment coring operations preferentially select high accumulation sites, i.e., those sites that have likely experienced sediment focusing rather than winnowing. This sampling bias is thought to at least partly explain why Th-normalized fluxes are higher than MARs at many sites. Beyond sampling bias, however, there is no agreement yet about a source region for the additional sediment [*Lyle et al.* 2005, 2007], although the Galapagos Spreading Centre and parts (but not all) of the Carnegie Ridge likely act as sources [*Kienast et al.*, 2007; *Singh et al.*, 2011].

[10] The accuracy of Th normalization depends on two fundamental assumptions. The first one is that the flux of scavenged  $^{230}\text{Th}$  to the seafloor equals the rate of  $^{230}\text{Th}$  production by  $^{234}\text{U}$  decay in seawater. The residence time of dissolved  $^{230}\text{Th}$  in the ocean is only a few decades [*Anderson et al.*, 1983]. Horizontal diffusion of dissolved  $^{230}\text{Th}$  and boundary scavenging are thus inherently limited. New measurements of dissolved  $^{230}\text{Th}$  in the water column of the Panama Basin region indeed show that lateral diffusion of dissolved  $^{230}\text{Th}$  into the Panama Basin region amounts to, at most, 15–30% of its in situ production [*Singh et al.*, 2013]. The findings of *Singh et al.* [2013] are consistent with earlier model studies [*Henderson et al.*, 1999; *Marchal et al.*, 2000; *Siddall et al.*, 2008] and sediment-trap observations [*Scholten et al.*, 2005; *Yu et al.*, 2001], collectively supporting the use of Th normalization. The second assumption is that scavenged  $^{230}\text{Th}$  concentrations are constant across different particle compositions and size classes. In laboratory experiments,  $^{230}\text{Th}$  has indeed shown high affinities to carbonate, opal, and manganese oxides [*Geibert and Usbeck*, 2004]. However,  $^{230}\text{Th}$  preferentially adheres to smaller particles [ $<10\text{ }\mu\text{m}$ ; *Kretschmer et al.*, 2010; *McGee et al.*, 2010]. This potentially leads to underestimating vertical flux in areas of lateral sediment redistribution on the seafloor, because smaller particles are transported preferentially to areas of sediment focusing. Nevertheless, in an area of

intense sediment redistribution, *McGee et al.* [2010] observed that the fidelity of  $^{230}\text{Th}$  normalization is not significantly compromised. The likely reason is that particles smaller than  $10\text{ }\mu\text{m}$  [*McCave and Hall*, 2006], or possibly even  $16\text{ }\mu\text{m}$  [*Law et al.*, 2008], move cohesively rather than as single grains. In the EEP, the particle grain-size effect [*Kretschmer et al.*, 2010; *McGee et al.*, 2010] and the effect of lateral diffusion [*Singh et al.*, 2013] would both bias flux estimates toward lower values.

[11] More research is needed to fully resolve the debate revolving around MARs and Th normalization and to further improve our understanding of Th systematics. Because errors in chronology greatly affect MAR values, but not Th-normalized fluxes, we consider Th normalization the more reliable of the two methods on the relatively short geologic timescales of interest here. We will refer to MAR-based estimates for completeness in the discussion below as well.

[12] In order to compare the sedimentary data to model predictions, we conduct a freshwater hosing experiment using the Earth system model LOVECLIM 1.2 [*Goosse et al.*, 2010] and quantify the response of SSTs, precipitation, wind field, and vertical velocities in the EEP to a shutdown of the AMOC in the North Atlantic. LOVECLIM 1.2 has been used extensively for past climate studies that require coupled multicentennial or multimillennial simulations and is thus well suited for the time period considered here. However, we note that its horizontal ocean resolution ( $3^\circ$  by  $3^\circ$ ) is not sufficient for a complete representation of the spatially complex equatorial current regime and that the strength of the tropical trade winds is underestimated compared to the observations.

## 4. Experimental Section

### 4.1. Core Sites

[13] Core ME0005-24JC was recovered at the base of the northern flank of the Carnegie ridge, underneath the equatorial front and close to the southern boundary of the EPWP (Figure 1 and Table 1). Cores V19-30 and TR163-31P were recovered from the southern flank of the Carnegie ridge underneath the cold tongue region. The present-day annual mean meridional SST gradient between ME0005-24JC and the other two sites amounts to  $\sim 3^\circ\text{C}$  (WOA09) [*Locarnini et al.*, 2010], and the ITCZ remains north of all sites year-round.

### 4.2. Thorium-232 and Organic Carbon Fluxes

[14] Total  $^{230}\text{Th}$ ,  $^{232}\text{Th}$ , and  $^{238}\text{U}$  activities of cores ME0005-24JC and TR163-31P were determined at the Woods Hole Oceanographic Institution (WHOI) and the University of British Columbia (UBC) by isotope dilution on an inductively coupled plasma mass spectrometer following total acid digestion of sediment samples equilibrated with  $^{229}\text{Th}$  and  $^{236}\text{U}$  spikes. Details and principles of the procedure can be found in *Choi et al.* [2001] and *François et al.* [2004]. Using these data, Th-normalized fluxes of bulk sediment and organic carbon (Corg) have been published previously [*Kienast et al.*, 2007]. Here we estimate  $^{232}\text{Th}$  flux by normalizing  $^{232}\text{Th}$  concentrations to  $^{230}\text{Th}$  following *François et al.* [2004, and references therein]. Data for core V19-30 are taken from *Hayes et al.* [2011, supplementary material].

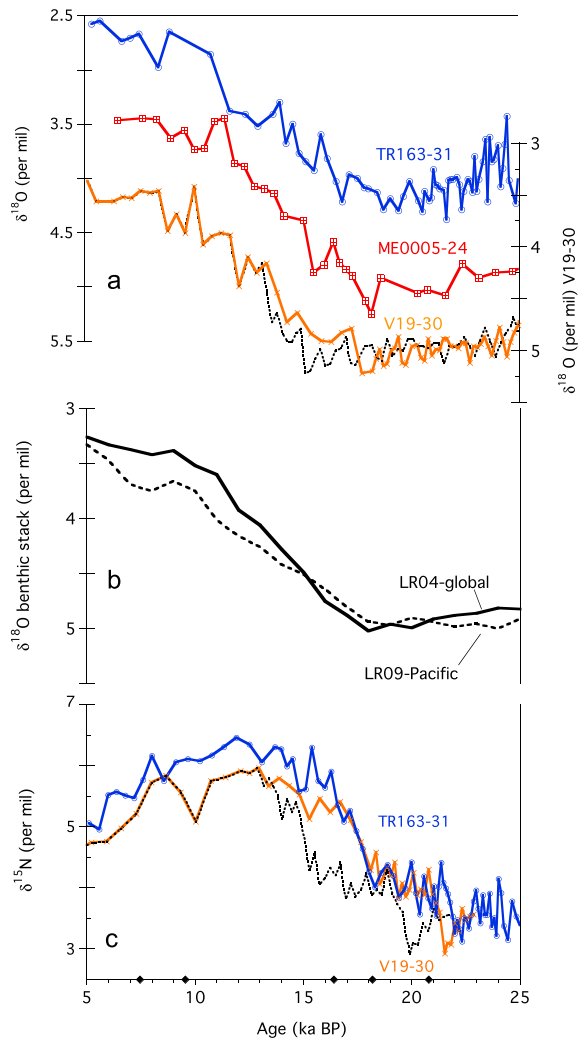


**Figure 2.** (a) Benthic  $\delta^{18}\text{O}$  records of the cores used in this study compared to (b) benthic  $\delta^{18}\text{O}$  stacks and (c)  $\delta^{15}\text{N}$  records. In Figures 2a and 2c, core V19-30 is plotted according to the original age model (dashed) [Koutavas and Sachs, 2008] and the adjusted age model (orange, this study). Benthic  $\delta^{18}\text{O}$  data of ME0005-24JC are from this study, and chronology is from Dubois *et al.* [2011]. Benthic  $\delta^{18}\text{O}$  data of TR163-31P and chronology are from Martin *et al.* [2002]. V19-30  $\delta^{18}\text{O}$  data are from Shackleton and Pisias [1985]. The global benthic stack (LR04, solid) [Lisiecki and Raymo, 2005] and the more recent Pacific stack (LR09, dashed) [Lisiecki and Raymo, 2009] are both shown in Figure 2b.  $\delta^{15}\text{N}$  data of core TR163-31P are from Dubois *et al.* [2011], and those of V19-30 are new to this study. Diamonds on the x axis are calibrated radiocarbon dates of ME0005-24JC from Dubois *et al.* [2011].

#### 4.3. Alkenone Unsaturation Ratios as a Proxy for SST

[15] All SST data discussed here have been published previously and are based on alkenone paleothermometry. Alkenone unsaturation ratios (expressed as the  $U^{K'}_{37}$  index) are converted to SST estimates based on the calibration of Prahl *et al.* [1988], which has recently been confirmed to relate  $U^{K'}_{37}$  to mean annual SSTs in the EEP most accurately [Kienast *et al.*, 2012]. SST data for TR163-31P are taken from

Dubois *et al.* [2009, 2011]. Data for ME0005-24JC are taken from Kienast *et al.* [2006] but shifted by  $+0.027 U^{K'}_{37}$  units (or  $0.8^\circ\text{C}$ ) to account for a laboratory offset between WHOI and Dalhousie (see Dubois *et al.* [2011] for details). Alkenone SST data of core V19-30 are taken from Koutavas and Sachs [2008]. A potential seasonal bias of alkenone-based SST estimates [Schneider *et al.*, 2010] will not be considered in this study.

#### 4.4. $\delta^{15}\text{N}$

[16] Bulk sedimentary  $\delta^{15}\text{N}$  measurements of all cores were carried out at the Pacific Centre for Isotopic and Geochemical Research at UBC. Data of cores ME0005-24JC and TR163-31P were previously published by Dubois *et al.* [2011], whereas data for core V19-30 are new to this study. An unexplained systematic offset was noted between the more recent data of V19-30 and those of TR163-31P and independently confirmed by reanalysis of selected samples of core TR163-31P. In light of the close proximity of these cores (Figure 1 and Table 1), we attribute this offset to instrument drift and added  $0.7\text{‰}$  to all  $\delta^{15}\text{N}$  values of V19-30.

#### 4.5. $\delta^{18}\text{O}$

[17] Stable oxygen isotope measurements of benthic foraminifera from core ME0005-24JC were performed at the Oregon State University College of Earth, Ocean, and Atmospheric Sciences (OSU/CEOAS) Stable Isotope Mass Spectrometer Facility using a Kiel III carbonate preparation device connected to a Thermo-Finnigan MAT-252 mass spectrometer. The data were corrected to the accepted PDB scale using an internal lab calcite standard (Wiley) and the international calcite standard NIST-8544 (NBS-19,  $\delta^{18}\text{O} = -2.20$ ). External precision (1 standard deviation) of the Wiley standard of similar weight to the foraminiferal samples was  $\pm 0.05$  per mil. Only  $\delta^{18}\text{O}$  of *Uvigerina* spp. ( $>150 \mu\text{m}$ ) are shown (Figure 2), but additional isotope data were generated and will be archived digitally with all other new data from this study. Benthic oxygen isotope data for cores TR163-31P and V19-30 are taken from Martin *et al.* [2002] and Shackleton and Pisias [1985], respectively.

#### 4.6. LOVECLIM Earth System Model Experiment for HS1

[18] LOVECLIM1.2 is a coupled ocean sea-ice atmosphere vegetation model [Goosse *et al.*, 2010]. The ocean component CLIO consists of an ocean general circulation model with a resolution of  $3^\circ$  by  $3^\circ$  and 20 levels in the vertical [Goosse *et al.*, 1999]. CLIO is coupled to a thermodynamic-dynamic sea-ice model. Mixing along isopycnals, as well as the effect of meso-scale eddies on transports, and mixing, and downsloping currents at the bottom of continental shelves are parameterized. The strength of diapycnal mixing is a function of seafloor topography as presented in Friedrich *et al.* [2011]. The atmospheric component (ECBilt) is a quasi-geostrophic potential vorticity model with three levels and a T21 horizontal resolution of  $5.625^\circ$  by  $5.625^\circ$ , extended by a parameterization of the ageostrophic terms. Due to the weakness of the Atlantic-Pacific moisture export, 8–15% of precipitation over the North Atlantic is redirected into the Pacific to maintain a stable AMOC under present-day conditions. The ocean, atmosphere, and sea-ice components are coupled by exchange of momentum, heat, and freshwater

**Table 2.** Previous and Revised Age-Tie Points for V19-30<sup>a</sup>

V19-30 (cm)	Previous Age (ka)	Revised Age (ka)
0	1	1
87	13	13
120	15.32	18.21
245	25.43	25.43

<sup>a</sup>Previous age-tie points are from Koutavas and Sachs [2008] and Koutavas (personal communication, 2010). The revised age-tie point at 120 cm used in this study was derived by aligning the benthic  $\delta^{18}\text{O}$  maxima of core V19-30 with the global LR04 stack [Lisiecki and Raymo, 2005].

fluxes. The vegetation model, VECODE [Brovkin *et al.*, 1997], computes the evolution of vegetation cover described as a fractional distribution of desert, tree, and grassland from local annual mean values of precipitation and temperature at the same resolution as ECBilt. Bottom moisture and soil properties are determined from a simple bucket model connected to a river runoff scheme.

[19] In a first step, the model was spun-up for 5000 years under Last Glacial Maximum (LGM) boundary conditions. The atmospheric  $\text{CO}_2$  concentration was prescribed to LGM values at 190 ppmv, and orbital parameters and continental ice sheets were chosen accordingly (see Menviel *et al.* [2008] for details). A major shutdown of the AMOC, mimicking conditions during HS1, was generated through freshwater (FW) hosing in the North Atlantic region between 50 and 70°N. FW-forcing is applied for 100 model years with an amplitude of 1 sverdrup (Sv) without salinity compensation [Stocker *et al.*, 2007]. It should be noted that the amount of FW is not intended to represent recorded sea level changes during Heinrich 1. The FW-forcing is idealized and has been chosen according to the model's AMOC sensitivity.

#### 4.7. Age Control

[20] The age model of ME0005-24JC has recently been updated, and is based on six radiocarbon dates between 0 and 20 ka B.P., and on correlating sedimentary features to the high-resolution  $\delta^{18}\text{O}$  ice EPICA record prior to 20 ka B. P. (scenario 1) [Dubois *et al.*, 2011]. The age model of core TR163-31P is taken from Martin *et al.* [2002]. It is based on a benthic  $\delta^{18}\text{O}$  record and its correlation to SPECMAP and on radiocarbon measurements on planktonic foraminifera from companion core TR163-31B. The benthic  $\delta^{18}\text{O}$  records of both cores agree well with the global benthic stack (LR04 [Lisiecki and Raymo, 2005]) and the more recent Pacific benthic stack (LR09-Pacific [Lisiecki and Raymo, 2009]; Figures 2a and 2b). The chronology of core V19-30, which covers the last four glacial-interglacial cycles, is based on tuning the deglaciation midpoints of the benthic  $\delta^{18}\text{O}$  record to an orbital tuning target [Shackleton *et al.*, 2000]. Importantly, an earlier study of deglacial SST gradients in the EEP [Koutavas and Sachs, 2008] used a slightly modified version of Shackleton's original chronology to establish the timing of the deglacial SST rise in the EEP (Table 2; Koutavas, personal communication, 2010). Careful examination of the stratigraphy of the last 25 ka in V19-30, however, reveals that this chronology does not agree in detail with either the chronologies of ME0005-24JC, TR163-31P, or the benthic stacks at the beginning of the last termination (Figure 2a, dashed), confirming that tuning of termination midpoints can exaggerate errors in  $\delta^{18}\text{O}$ -based chronologies

[Lisiecki and Raymo, 2009]. We have therefore adjusted the chronology of V19-30 by aligning the glacial  $\delta^{18}\text{O}$  maximum of V19-30 to that of LR04 by shifting a single age-fix point (Figure 2a, solid, and Table 2). This adjustment leads to a much closer agreement between the benthic  $\delta^{18}\text{O}$  record of

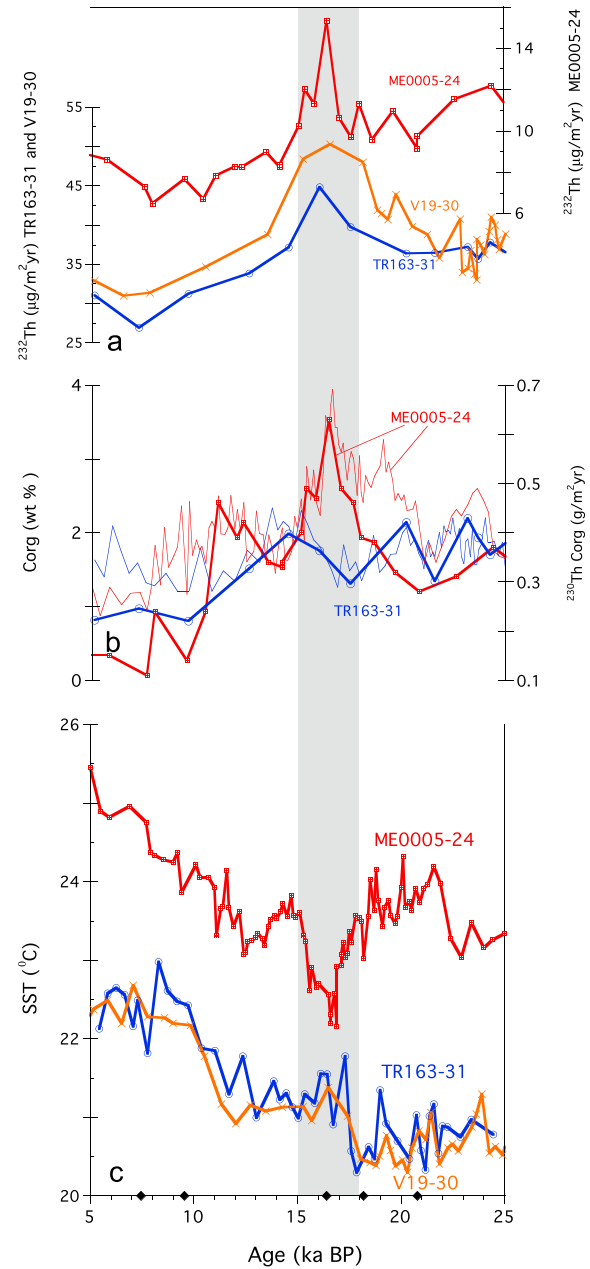


**Figure 3.** (a)  $^{230}\text{Th}$ -normalized fluxes of the continental isotope  $^{232}\text{Th}$  in cores ME0005-24JC (red), TR163-31P (blue), and V19-30 (orange; note different y scales). (b)  $^{230}\text{Th}$ -normalized fluxes of organic carbon of cores ME0005-24JC (red) and TR163-31P (blue) taken from Kienast *et al.* [2007]. Organic carbon weight percentages are given in thin lines. (c) Sea surface temperature records of cores ME0005-24JC (red) [Kienast *et al.*, 2006], V19-30 (orange, on revised age scale) [Koutavas and Sachs, 2008], and TR163-31P (blue) [Dubois *et al.*, 2011]. Diamonds on the x axis are calibrated radiocarbon dates of ME0005-24JC from Dubois *et al.* [2011].



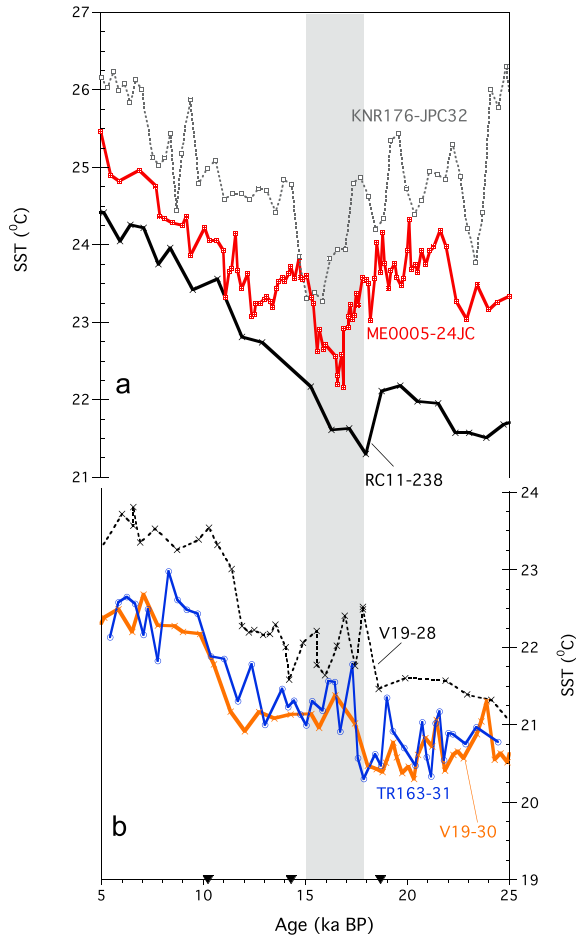


**Figure 4.** Alkenone SST records from (a) the Eastern Pacific Warm Pool (KNR-176-JPC32) and close to the equator (ME0004-24JC and RC11-238) compared to alkenone SST records from (b) the cold tongue region (V19-28, V19-30, and TR163-31P). Data and age model of KNR-176-JPC32 are taken from *Pahnke et al.* [2007], and data and age models of V19-28 and RC11-238 are from *Koutavas and Sachs* [2008].

V19-30 and the other two cores (Figures 2a and 2b). Close agreement between the benthic  $\delta^{18}\text{O}$  signal recorded at these sites is expected given their proximity, irrespective of absolute age or spatial and temporal complexities associated with the propagation of the glacioeustatic  $\delta^{18}\text{O}$  signal [*Friedrich and Timmermann*, 2012; *Lisiecki and Raymo*, 2009; *Skinner and Shackleton*, 2005]. The accuracy of the chronologies for the LGM and before, and for the Holocene is beyond the scope of our discussion of deglacial changes and will not be evaluated here.

[21] The Pacific benthic  $\delta^{18}\text{O}$  stack lags the Atlantic  $\delta^{18}\text{O}$  stack (not shown) at the end of the last deglaciation [*Lisiecki and Raymo*, 2009]. To be consistent with previous studies, we chose not to update all core chronologies to the more recent stack. This choice does not affect the conclusions below since we are examining the phasing between events recorded in nearby cores, separated by only  $\sim 3.6^\circ$ .

[22] Two independent lines of evidence support our adjustment to the original chronologies of V19-30 presented by *Shackleton* [2000] and *Koutavas and Sachs* [2008]. First, the above revision of the age model of V19-30 leads to closer

agreement of linear sedimentation rates at the two nearby sites V19-30 and TR163-31P (not shown). Second, based on the revised chronology, the timing of the deglacial  $\delta^{15}\text{N}$  increase at site V19-30 is now synchronous to that of neighboring TR163-31P (Figure 2c), as expected for two cores within a few tens of kilometers of each other in the EEP [*Tesdal et al.*, 2013]. Furthermore, the timing of the deglacial  $\delta^{15}\text{N}$  in V19-30 now agrees with the absolute age of this increase, which has been established in a suite of high-resolution  $\delta^{15}\text{N}$  records from the EEP, and is necessitated by a common forcing mechanism of this regionally coherent  $\delta^{15}\text{N}$  increase [cf. *Robinson et al.*, 2009; *Dubois and Kienast*, 2011].

## 5. Results

### 5.1. SST Patterns in the EEP

[23] Just north of the equator (ME0005-24JC), SSTs drop sharply by  $\sim 1^\circ\text{C}$  during HS1 (Figure 3c). South of the equator, however, in the cold tongue, cores V19-30 and TR163-31P reveal a significant warming just at the onset of HS1 (Figure 3c). For core V19-30, the warming during HS1 is a direct result of the revised chronology (section 4.6). However, another nearby site in the cold tongue, V19-28 [*Koutavas and Sachs*, 2008], also shows relatively warm SSTs during HS1, supporting the revised chronology of V19-30 (Figure 4b and Table 3). Additional evidence for a relative warming during HS1 in the cold tongue region comes from site 106KL further south in the Peru upwelling region [ $\sim 12^\circ\text{S}$ , *Rein et al.*, 2005]. Similar to site ME0005-24JC, lower SSTs during HS1 are also observed at sites RC11-238 [*Koutavas and Sachs*, 2008], KNR176-JPC32 [*Pahnke et al.*, 2007] (see Figure 4 and Table 3), and V19-27 [*Koutavas and Sachs*, 2008]. Taken together, these records suggest that there are two types of SST responses during HS1 in the EEP as inferred from alkenone paleothermometry: A relative cooling in the EPWP and close to the equator (KNR176-JPC32, ME0005-24JC, V19-27, and RC11-238) and a warming in the cold tongue region south of  $2^\circ\text{S}$  (V19-30, TR163-31P, V19-28, and 106KL).

[24] A consequence of the different SST responses in both areas is a reduction of the meridional SST gradient. The SST gradient between site ME0005-24JC and sites V19-30 and TR163-31P is reduced from  $\sim 3^\circ\text{C}$  during the LGM to  $\sim 1^\circ\text{C}$  or less during HS1 (Figure 3c). At no other time interval over the last 25 ka was the gradient as small as during HS1. The SST signals during HS1 reported here contrast with a uniform warming of the EEP following a Northern Hemisphere timing inferred previously [*Koutavas and Sachs*, 2008].

### 5.2. Thorium-232

[25] Thorium-232 fluxes (Figure 3a) are highest in cores V19-30 and TR163-31P ( $30\text{--}50\text{ mg/m}^2\text{yr}$ ), which are located closer to the continent, and lower at site ME0005-24JC ( $8\text{--}16\text{ mg/m}^2\text{yr}$ ). All three cores show slightly elevated  $^{232}\text{Th}$  fluxes during glacial stage 2 compared to

**Table 3.** Additional Sites Shown in Figure 4

	Longitude	Latitude	Reference
KNR176-JPC32	$77^\circ 57.80'\text{W}$	$4^\circ 39.99'\text{N}$	<i>Pahnke et al.</i> [2007]
RC11-238	$85^\circ 49'\text{W}$	$1^\circ 31'\text{S}$	<i>Koutavas and Sachs</i> [2008]
V19-28	$84^\circ 39'\text{W}$	$2^\circ 22'\text{S}$	<i>Koutavas and Sachs</i> [2008]

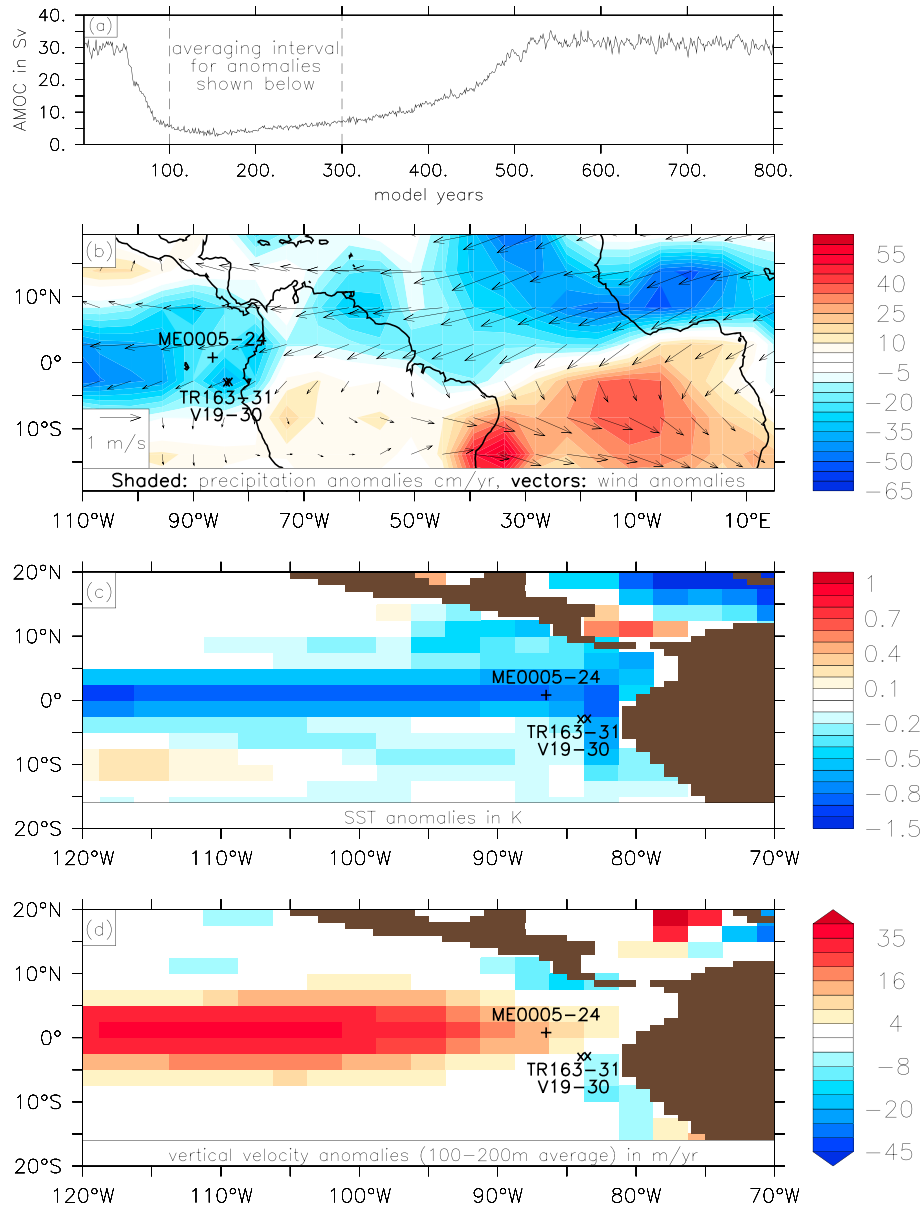


**Figure 5.** (a) Time series of the Atlantic meridional overturning circulation (AMOC) in sverdrup. The AMOC is defined as the maximum of the overturning in the North Atlantic north of 30°N. (b) Precipitation anomalies in cm/yr (shaded) and surface wind anomalies (vectors). (c) Sea surface temperature (SST) anomalies in kelvin. (d) Vertical velocity anomalies averaged between 100 and 200 m water depth in m/yr. All anomalies are calculated with respect to the mean state prior to freshwater forcing. The averaging interval for all anomalies is depicted in Figure 5a.

those during the Holocene (Figure 3a), akin to the overall glacial-interglacial trend observed further west in the central equatorial Pacific (140°W and 110°W) [McGee *et al.*, 2007; Winckler *et al.*, 2008]. This glacial-interglacial  $^{232}\text{Th}$  decrease in our cores is more pronounced when expressed in MAR estimates (not shown). In addition, the far eastern EEP cores studied here show a clear  $^{230}\text{Th}$ -normalized  $^{232}\text{Th}$  flux maximum during HS1 (Figure 3a). A deglacial maximum in  $^{230}\text{Th}$ -normalized  $^{232}\text{Th}$  fluxes is also observed at sites RC11-238 [Bradtmiller *et al.*, 2006, supplementary data] and TR163-19P [Carrière-Garwood *et al.*, 2012]. The deglacial maximum  $^{232}\text{Th}$  is also evident from  $^{232}\text{Th}$ -MAR estimates at site ME0005-24JC (not shown). Thorium-232

MAR estimates are higher during the LGM, not HS1, at sites V19-30 and TR163-31P (not shown). We posit, however, that these peak MARs during the LGM are caused in part by the difficulty in assigning absolute age-fix points based on benthic  $\delta^{18}\text{O}$  for the times before the LGM at sites V19-30 and TR163-31P.

### 5.3. Corg Fluxes

[26]  $^{230}\text{Th}$ -normalized Corg fluxes are elevated during the LGM and lower during the Holocene (Figure 3b), which is now a well-recognized pattern in a variety of records of EEP productivity covering this time interval, and also evident in MAR-based flux estimates [e.g., Martinez and

Robinson, 2010; Kienast et al., 2007, Lyle et al., 1988, 2002]. Corg concentrations and fluxes are maximal at site ME0005-24JC when SSTs are minimal during HS1. This Corg peak at site ME0005-24JC is corroborated by MAR estimates (not shown). Interestingly, Th-normalized Corg fluxes at the cold tongue site TR163-31P show a slight intermittent minimum at that time (Figure 3b). Note that this feature is not evident in Corg MARs.

#### 5.4. LOVECLIM 1.2

[27] In response to the AMOC shutdown, northeasterly trade wind strength increases and precipitation decreases in the far eastern EEP (Figure 5b). The strengthening of the northeasterly trade winds is related to the cooling of the Northern Hemisphere and the associated southward shift of the ITCZ. Drier conditions are not only observed in the EEP but also in Northern South America and the Sahel region in Africa (Figure 5b). The spatial pattern of precipitation observed here is consistent with recent results of a study comparing 11 models [Kageyama et al., 2013]. During HS1, SSTs drop by  $\sim 1$  K ( $=1^\circ\text{C}$ ) at site ME0005-24JC and along the entire equatorial upwelling zone (Figure 5c). A more modest cooling ( $0.5$ – $0.2^\circ\text{C}$ ) is observed at sites TR163-31P and V19-30 in the cold tongue in LOVECLIM. This cooling is different from the warming observed in alkenone-based SST records at these sites (Figure 3c). Vertical velocity (i.e., upwelling) anomalies averaged for the base of the thermocline (100–200 m) display a dipole in the study area (Figure 5d). At site ME0005-24JC, vertical velocities increase by  $\sim 16$  m/yr, but they decrease slightly at the two southern sites V19-30 and TR163-31P. However, the locations of the southern sites correspond to the location where the simulated upwelling anomalies reverse their sign, rendering the results less certain.

## 6. Discussion

### 6.1. SST Patterns

[28] Our alkenone-based SST reconstructions show cooling in the equatorial region and net warming south of the equator, consistent with a near collapse of the meridional SST gradient during HS1 (Figure 3c). This is in excellent agreement with previous Coupled General Circulation Model experiments [Merkel et al., 2010; Timmermann et al., 2007b; Zhang and Delworth, 2005] that show a similar dipole SST pattern in response to a weakening of the AMOC. However, LOVECLIM (Figure 5c) exhibits a much more symmetric structure across the equator and no net warming south of the equator. It is possible that this lack of warming in LOVECLIM is related to its lack of horizontal resolution ( $3^\circ$  by  $3^\circ$ ) and thus insufficient representation of the equatorial current dynamics. However, we also note that in a regional modeling experiment, the south equatorial Pacific warming was found to be seasonally dependent and the SST dipole most strongly developed from January to May [Xie et al., 2008, Figure 11]. Given the seasonal sensitivity in model experiments [Xie et al., 2008], in addition to potential seasonal effects on alkenone-based SST reconstructions [Schneider et al., 2010], and the presence of deglacial background trends, we acknowledge that it is still difficult to constrain which group of model simulations mentioned above is most consistent with the paleo-data evidence presented here.

[29] The potential effects of the reconstructed weakening of the meridional EEP SST gradient are a reduction in the strength of the annual cycle in the EEP and increased ENSO variability, as discussed extensively by Timmermann et al. [2007b] and Merkel et al. [2010].

### 6.2. Continental Input to the EEP

[30] Thorium-232 fluxes peak on both sides of the equator during the early deglaciation (Figure 3a), suggesting that the same “continental response” acted on both sides of the equator. In analyses of more remote core sites,  $^{232}\text{Th}$  fluxes have been interpreted as a tracer for dust [Winckler et al., 2008; McGee et al., 2007; Anderson et al., 2006]. However, at our core sites, continental input could be either hemipelagic (i.e., terrestrial, riverine material that escaped the continental margin) or atmospheric. Singh et al. [2011] present average Holocene and glacial  $^{232}\text{Th}$  fluxes in a set of 13 cores from the EEP and find a sharp decline in continental material with increasing distance from the margin. These authors find that dust dominates over riverine detrital input 300 km away from the continental margin. This implies that at site ME0005-24JC, located roughly 600 km offshore, continental material is predominantly atmospherically transported, whereas sites V19-30 and TR163-31P ( $\sim 300$  km offshore) are probably affected by both atmospheric and hemipelagic sources. A recent study of grain-size distributions and clay-mineral compositions of EEP surface sediments found that “wind is the dominant transport agent and eolian material is the dominant terrigenous component west of the Peru-Chile Trench south of  $\sim 5^\circ\text{S}$ ” [Saukel et al., 2011], which is slightly to the south of sites V19-30 and TR163-31P (at  $3.6^\circ\text{S}$ ). Boven and Rea [1998] argued based on inorganic grain-size analyses that both eolian and hemipelagic sources contribute to the terrigenous sediment component at site TR163-31B (the companion core of TR163-31P investigated here) during the deglaciation. We thus interpret  $^{232}\text{Th}$  as predominantly of eolian origin at site ME0005-24JC and mixed eolian and hemipelagic origin at sites V19-30 and TR163-31P. Further support for an atmospheric dust deposition event during HS1 in the EEP comes from site RC11-238 ( $1.5^\circ\text{S}$ ,  $85.8^\circ\text{W}$ ) [Bradtmiller et al., 2006, supplementary data] and site TR163-19P ( $2.3^\circ\text{N}$ ,  $90.9^\circ\text{W}$ ) [Carrière-Garwood et al., 2012]. The  $^{230}\text{Th}$ -normalized  $^{232}\text{Th}$  flux maximum during the deglaciation (Figure 3a) is also apparent in  $^{232}\text{Th}$ -MARs (not shown) in core ME0005-24JC. However, the  $^{232}\text{Th}$ -record at sites TR163-31 and V19-30 is slightly more ambiguous. While  $^{230}\text{Th}$ -normalized fluxes of  $^{232}\text{Th}$  in these cores support the notion of peak continental input during HS1 (Figure 3a), possibly indicative of peak atmospheric input at that time, MARs (not shown) would suggest highest levels of continental input during the LGM.

[31] In the LOVECLIM experiment, precipitation upstream of the three core locations decreases by 10–20% in northern South America and Meso America (Figure 5b), which is generally consistent with drier conditions inferred from Lake records in Colombia [Hessler et al., 2010] and Central America [Hodell et al., 2008], as well as with higher sea surface salinity in the northern EEP [Leduc et al., 2007]. LOVECLIM simulates an even larger precipitation decrease ( $>50\%$ ) in the Sahel region (Figure 5b). In northern South America and Meso America, the relative decrease in simulated bottom moisture (not shown)—a major driver of dust



release from the soil—is of the same magnitude as the precipitation decrease. Together with increased NE trade winds in the study area (Figure 5b), LOVECLIM modeling results are consistent with increased atmospheric dust deposition during HS1 inferred from  $^{232}\text{Th}$  fluxes.

[32] A southward shift of the ITCZ is a consistent response to cooling in the North Atlantic in climate models [Deplazes *et al.*, 2013; Merkel *et al.*, 2010; Timmermann *et al.*, 2007b; Zhang and Delworth, 2005; Broccoli *et al.*, 2006; Chiang and Bitz, 2005]. A migration of the mean ITCZ to its southernmost position during HS1 would have placed site ME0005-24JC, and possibly also sites V19-30 and TR163-31P, to the north of it, at least during part of the year, exposing these locations to higher Northern Hemisphere dust loads. Dryness in central America [Hodell *et al.*, 2008] could have provided a proximal dust source to the EEP. In addition, the slowdown of the AMOC appears to have caused massive drying in the Sahel region of northern Africa [Mulitza *et al.*, 2008], which could have served as an additional, more distal dust source to the EEP. Observations over the last century reveal that low SSTs in the North Atlantic are associated with increased dust delivery to the North Atlantic due to drying of the Sahara and Sahel regions [Wang *et al.*, 2012]. It is well known from direct observations that African dust periodically reaches as far as the Caribbean [Prospero *et al.*, 1970; Prospero and Lamb, 2003; Liu *et al.*, 2008], and time series over the last 38 years indicate a strong statistical link between southward movements of the ITCZ and increased dust loads in the Caribbean during winter [Doherty *et al.*, 2012]. Model evidence suggests that African dust reaches the EEP even under modern conditions (CCSM-3) [Mahowald, 2007]. It is thus plausible that African dust reached the EEP during HS1 and contributed to the large fluxes observed in our cores. While it is difficult to link past movements of the ITCZ to geologic time series of dust flux, the weakened meridional SST gradient and the increase in detrital fluxes north and south of the equator are both consistent with a southward shift of ITCZ during HS1 in the far eastern EEP. This interpretation is consistent with the pronounced southward shift of the ITCZ during peak Heinrich events inferred from the Cariaco Basin [Deplazes *et al.*, 2013] (however, for a different view, see Xie and Marcantonio [2012]).

### 6.3. Productivity and Carbon Export

[33] Intensified NE trades during HS1 (Figure 5b) are related to increased Ekman divergence at the equator, lower SSTs, and higher export production at and north of the equatorial front. However, south of the equator a warming of the cold tongue, as seen in the paleo SST reconstructions (Figure 3c), implies that weakened SE trades [Timmermann *et al.*, 2007a] reduced upwelling of cooler, nutrient rich subsurface waters and thus reduced surface productivity.

[34] Vertical velocity anomalies simulated by LOVECLIM 1.2 indeed show an increase to the north of the equator and a slight decrease to the south of it during HS1 (Figure 5d). Consistent with this, elevated Corg fluxes are observed at several sites in the northern EEP during HS1 (Figure 3b) [Martinez and Robinson, 2010; Kienast *et al.*, 2006; Kienast *et al.*, 2007]. South of the equator, however, we observe an intermittent low in Corg fluxes at site TR163-31P (Figure 3b). While we note that this intermittent low is represented only

by a few samples (and not evident in MAR-based estimates), it is consistent with LOVECLIM model results (Figure 5d) and could suggest that upwelling and export production may have been somewhat lower to the south of the equator during the HS1 maxima in production north of the equator.

[35] Export production in the EEP is thought to be controlled by wind-driven upwelling along the equatorial divergence or, alternatively, preformed nutrient content of the Equatorial Undercurrent (EUC), which feeds upwelling and is ultimately sourced from the Southern Ocean. Because the EEP is Fe:Si colimited under modern conditions [e.g., Coale *et al.*, 1996; Brzezinski *et al.*, 2011, Dugdale *et al.*, 2011], an increase in the ratio of Fe and Si to nitrogen and phosphorous (compared to today) is required to increase export productivity by either mechanism. There is strong evidence for enhanced nutrient content of subsurface EUC waters during the deglacial period based on  $\delta^{13}\text{C}$  records of surface- and thermocline-dwelling foraminifera [Spero and Lea, 2002; Pena *et al.*, 2008]. In addition, residual  $\delta^{15}\text{N}$  records (i.e., nitrate utilization records from which the regional denitrification overprint as been removed) suggest that relative nitrate utilization was minimal during the HS1 and Younger Dryas (YD) stadials [Robinson *et al.*, 2009], consistent with nitrate being abundantly available during those time intervals. Minimal SSTs and maximal continental fluxes during HS1 (Figure 3), together with modeling evidence for intensified NE trades (Figure 5b), are thus consistent with peak export productivity in the northern EEP during the early deglaciation caused by increased upwelling and a release from Fe limitation. Elevated Corg and opal fluxes [Dubois *et al.*, 2011, Hayes *et al.*, 2011; Lyle *et al.*, 2002, Lyle *et al.*, 1988] and heavier  $\delta^{13}\text{C}$  values [Pena *et al.*, 2008] also characterize previous deglaciations, possibly implying that this mechanism is characteristic of the EEP during terminations. However, Corg and biogenic opal maxima do not always occur in the same depth interval within individual records [Kienast *et al.*, 2007], leaving the possibility that the productivity record in the EEP is influenced by additional mechanisms not yet understood.

## 7. Summary and Conclusions

[36] Sea surface temperature records spanning the last 25,000 years in the EEP reveal that SSTs during HS1 dropped in the equatorial upwelling zone, i.e., at and north of the equator, whereas the surface ocean warmed in the cold tongue region to the south of the equator. This led to a significant reduction of the cross-equatorial SST gradient in the EEP when meridional overturning circulation was reduced in the North Atlantic. This observation is consistent with predictions based on several models.

[37] Input of inorganic continental material is maximal at both sides of the equator during HS1, and we suggest that a large fraction of it was atmospheric dust. This observation is supported by modeling results that show decreased precipitation and enhanced northeasterly trade winds upstream of the core sites, which would increase dust mobilization from soils. Dust input is the critical ingredient to relieve Fe:Si colimitation, which affects the EEP under modern conditions. Together with increased northeasterly trade wind-driven upwelling and a higher preformed nutrient content during the deglaciation, dust input sets the stage for a large export production event in the northern EEP during the last deglaciation.

[38] **Acknowledgments.** We gratefully acknowledge constructive reviews by Mitchell Lyle and one anonymous reviewer, which helped to improve and clarify the manuscript. We also wish to acknowledge fruitful discussions with Athanasios Koutavas, Claire Normandeau, Kathy Gordon, Maureen Soon, Alan Fleer, and Susan Brown-Leger provided invaluable technical assistance. Core material was provided by the Core Repositories of Oregon State University (supported by NSF grant OCE97-12024) and Rhode Island (supported by NSF grant OCE-9102410). This work was supported by grants from the Canadian Foundation for Climate and Atmospheric Sciences (CFCAS), the Canadian Institute for Advanced Research (CIFAR), the Natural Sciences and Engineering Research Council (NSERC), Canada and the National Science Foundation (NSF), USA. A. Timmermann and T. Friedrich were supported by NSF grant 1010869. This is IPRC publication 1002 and SOEST publication 8980.

## References

- Anderson, R. F., M. P. Bacon, and P. G. Brewer (1983), Removal of  $^{230}\text{Th}$  and  $^{231}\text{Pa}$  from the open ocean, *Earth Planet. Sci. Lett.*, **62**(1), 7–23, doi:10.1016/0012-821X(83)90067-5.
- Anderson, R. F., M. Q. Fleischer, and Y. Lao (2006), Glacial-interglacial variability in the delivery of dust to the central equatorial Pacific, *Earth Planet. Sci. Lett.*, **242**, 406–414.
- Bacon, M. P. (1984), Glacial to interglacial changes in carbonate and clay sedimentation in the Atlantic Ocean estimated from  $^{230}\text{Th}$  measurements, *Isot. Geosci.*, **2**, 97–111.
- Boven, K. L., and D. K. Rea (1998), Partitioning of eolian and hemipelagic sediment in eastern equatorial Pacific core TR163-31B and the late Quaternary climate of the northern Andes, *J. Sediment. Res.*, **68**(5), 850–855.
- Bradt Miller, L. I., R. F. Anderson, M. Q. Fleischer, and L. H. Burckle (2006), Diatom productivity in the Equatorial Pacific Ocean from the Last Glacial Maximum to the present: A test of the silicic acid leakage hypothesis, *Paleoceanography*, **21**, doi:10.1029/2006PA001282.
- Broccoli, A. J., K. A. Dahl, and R. J. Stouffer (2006), Response of the ITCZ to Northern Hemisphere cooling, *Geophys. Res. Lett.*, **33**, L01702, doi:10.1029/2005/GL024546.
- Broecker, W. (2008), Excess sediment  $^{230}\text{Th}$ : Transport along the sea floor or enhanced water column scavenging?, *Global Biogeochem. Cycles*, **22**, GB1006, doi:10.1029/2007GB003057.
- Brovkin, V., A. Ganopolski, and Y. Svirezhev (1997), A continuous climate-vegetation classification for use in climate-biosphere studies, *Ecol. Model.*, **101**, 251–261.
- Brzezinski, M. A., et al. (2011), Co-limitation of diatoms by iron and silicic acid in the equatorial Pacific, *Deep Sea Res., Part II*, **58**, 493–511.
- Carrière-Garwood, J., S. S. Kienast, and P. S. Hill (2012), Evidence of dust deposition in a core from the Eastern Equatorial Pacific on glacial-interglacial timescales paper presented at AGU Fall Meeting (PP 21C-03), San Francisco, USA.
- Chavez, F. P., and R. T. Barber (1987), An estimate of new production in the equatorial Pacific, *Deep Sea Res.*, **34**, 1229–1243.
- Chiang, J., and C. Bitz (2005), Influence of high latitude ice cover on the marine Intertropical Convergence Zone, *Clim. Dyn.*, **25**, 477–496, doi:10.1007/s00382-005-0040-5.
- Choi, M. S., R. Francois, K. Sims, M. P. Bacon, S. Brown-Leger, A. P. Fleer, L. Ball, D. Schneider, and S. Pichat (2001), Rapid determination of  $^{230}\text{Th}$  and  $^{231}\text{Pa}$  in seawater by desolvated micro-nebulization inductively coupled plasma magnetic sector mass spectrometry, *Mar. Chem.*, **76**, 99–112.
- Coale, K. H., et al. (1996), A massive phytoplankton bloom induced by an ecosystem-scale iron fertilization experiment in the equatorial Pacific Ocean, *Nature*, **383**, 495–501.
- Deplazes, G., et al. (2013), Links between tropical rainfall and North Atlantic climate during the last glacial period, *Nat. Geosci.*, **6**(3), 213–217.
- Doherty, O. M., N. Riemer, and S. Hameed (2012), Control of Saharan mineral dust transport to Barbados in winter by the Intertropical Convergence Zone over West Africa, *J. Geophys. Res.*, **117**, D19117, doi:10.1029/2012JD017767.
- Dubois, N., and M. Kienast (2011), Spatial reorganization in the equatorial divergence in the eastern tropical Pacific during the last 150 kyr, *Geophys. Res. Lett.*, **38**, L16606, doi:10.1029/2011GL048325.
- Dubois, N., and N. C. Mitchell (2012), Large-scale sediment redistribution on the equatorial Pacific seafloor, *Deep Sea Res., Part I*, **69**, 51–61, doi:10.1016/j.dsr.2012.07.006.
- Dubois, N., M. Kienast, C. Normandeau, and T. D. Herbert (2009), Eastern equatorial Pacific cold tongue during the Last Glacial Maximum as seen from alkenone paleothermometry, *Paleoceanography*, **24**, PA4207, doi:10.1029/2009PA001781.
- Dubois, N., M. Kienast, S. Kienast, C. Normandeau, S. E. Calvert, T. D. Herbert, and A. Mix (2011), Millennial-scale variations in hydrography and biogeochemistry in the eastern equatorial Pacific over the last 100 kyr, *Quat. Sci. Rev.*, **30**, 210–233.
- Duce, R. A., et al. (1991), The atmospheric input of trace species to the world ocean, *Global Biogeochem. Cycles*, **5**(3), 193–259, doi:10.1029/91GB01778.
- Dugdale, R., F. Chai, R. Feely, C. Measures, A. Parker, and F. Wilkerson (2011), The regulation of equatorial Pacific new production and  $\text{pCO}_2$  by silicate-limited diatoms, *Deep Sea Res., Part II*, **58**, 477–492.
- Fiedler, P. C., and L. D. Talley (2006), Hydrography of the eastern tropical Pacific: A review, *Prog. Oceanogr.*, **69**, 143–180.
- Francois, R., M. Frank, M. M. Rutgers van der Loeff, and M. P. Bacon (2004),  $^{230}\text{Th}$  normalization: An essential tool for interpreting sedimentary fluxes during the late Quaternary, *Paleoceanography*, **19**, PA1018, doi:10.1029/2003PA000939.
- Francois, R., et al. (2007), Comment on “Do geochemical estimates of sediment focusing pass the sediment test in the equatorial Pacific” by Lyle et al., *Paleoceanography*, **22**, PA1217, doi:10.1029/2005PA001235.
- Friedrich, T., A. Timmermann, T. Decloedt, D. S. Luther, and A. Mouchet (2011), The effect of topography-enhanced diapycnal mixing on ocean and atmospheric circulation and marine biogeochemistry, *Ocean Modell.*, **39**, 262–274.
- Friedrich, T., and A. Timmermann (2012), Millennial-scale glacial meltwater pulses and their effect on the spatiotemporal benthic  $\delta^{18}\text{O}$  variability, *Paleoceanography*, **27**, doi:10.1029/2012PA002330.
- Geibert, W., and R. Usbeck (2004), Adsorption of thorium and protactinium onto different particle types: Experimental findings, *Geochim. Cosmochim. Acta*, **68**(7), 1489–1501.
- Goosse, H., E. Deleersnijder, T. Fichefet, and M. England (1999), Sensitivity of a global coupled ocean-sea ice model to the parameterization of vertical mixing, *J. Geophys. Res.*, **104**(C6), 13,681–13,695.
- Goosse, H., et al. (2010), Description of the Earth system model of intermediate complexity LOVECLIM version 1.2, *Geosci. Model Dev.*, **3**(2), 603–633, doi:10.5194/gmd-3-603-2010.
- Hayes, C. T., R. F. Anderson, and M. Q. Fleisher (2011), Opal accumulation rates in the equatorial Pacific and mechanisms of deglaciation, *Paleoceanography*, **26**, PA1207, doi:10.1029/2010PA002008.
- Henderson, G. M., C. Heinze, R. F. Anderson, and A. M. E. Winguth (1999), Global distribution of the  $^{230}\text{Th}$  flux to ocean sediments constrained by GCM modeling, *Deep Sea Res., Part I*, **46**, 1861–1893.
- Hessler, I., et al. (2010), Millennial-scale changes in vegetation records from tropical Africa and South America during the last glacial, *Quat. Sci. Rev.*, **29**(21–22), 2882–2899, doi:10.1016/j.quascirev.2009.11.029.
- Hodell, D. A., et al. (2008), An 85-ka record of climate change in lowland Central America, *Quat. Sci. Rev.*, **27**(11–12), 1152–1165, doi:10.1016/j.quascirev.2008.02.008.
- Jickells, T. D., et al. (2005), Global iron connections between desert dust ocean biogeochemistry, and climate, *Science*, **308**, 67–71.
- Joly, M., and A. Voldoire (2009), Influence of ENSO on the West African Monsoon: Temporal aspects and atmospheric processes, *J. Clim.*, **22**(12), 3193–3210, doi:10.1175/2008jcli2450.1.
- Kageyama, M., U. Merkel, B. Otto-Bliesner, M. Prange, A. Abe-Ouchi, G. Lohmann, D. M. Roche, J. Singarayer, D. Swingedouw, and X. Zhang (2013), Climatic impacts of fresh water hosing under Last Glacial Maximum conditions a multi-model study, *Clim. Past Discuss.*, **8**, 3831–3869.
- Kienast, M., S. S. Kienast, S. E. Calvert, T. I. Eglinton, G. Mollenhauer, R. François, and A. C. Mix (2006), Eastern Pacific cooling and Atlantic overturning circulation during the last deglaciation, *Nature*, **443**, 846–849, doi:10.1038/nature05222.
- Kienast, S. S., M. Kienast, A. C. Mix, S. E. Calvert, and R. François (2007), Thorium-230 normalized particle flux and sediment focusing in the Panama Basin region during the last 30,000 years, *Paleoceanography*, **22**, PA2213, doi:10.1029/2006PA001357.
- Kienast, M., G. MacIntyre, N. Dubois, S. Higginson, C. Normandeau, C. Chazen, and T. D. Herbert (2012), Alkenone unsaturation in surface sediments from the eastern equatorial Pacific: Implications for SST reconstructions, *Paleoceanography*, **27**, PA1210, doi:10.1029/2011PA002254.
- Koutavas, A., and J. P. Sachs (2008), Northern timing of deglaciation in the eastern equatorial Pacific from alkenone paleothermometry, *Paleoceanography*, **23**, PA4205, doi:10.1029/2008PA001593.
- Kretschmer, S., W. Geibert, M. M. Rutgers van der Loeff, and G. Mollenhauer (2010), Grain size effects on  $^{230}\text{Th}$  inventories in opal-rich and carbonate-rich marine sediments, *Earth Planet. Sci. Lett.*, **294**, 131–142, doi:10.1016/j.epsl.2010.03.021.
- Law, B. A., P. S. Hill, T. G. Milligan, K. J. Curran, P. L. Wiberg, and R. A. Wheatcroft (2008), Size sorting of fine-grained sediments during erosion: Results from the western Gulf of Lions, *Cont. Shelf Res.*, **28**(15), 1935–1946, doi:10.1016/j.csr.2007.11.006.
- Lea, D. W., D. K. Pak, C. L. Belanger, H. J. Spero, M. A. Hall, and N. J. Shackleton (2006), Paleoclimate history of Galapagos surface waters over the last 135,000 yr, *Quat. Sci. Rev.*, **25**, 1152–1167, doi:10.1016/j.quascirev.2005.11.010.

- Leduc, G., L. Vidal, K. Tachikawa, F. Rostek, C. Sonzogni, L. Beaufort, and E. Bard (2007), Moisture transport across Central America as a positive feedback on abrupt climatic changes, *Nature*, 445(7130), 908–911, doi:10.1038/nature05578.
- Lisiecki, L. E., and M. E. Raymo (2005), A Pliocene-Pleistocene stack of 57 globally distributed benthic  $\delta^{18}\text{O}$  records, *Paleoceanography*, 20, PA1003, doi:10.1029/2004PA001071.
- Lisiecki, L. E., and M. E. Raymo (2009), Diachronous benthic  $\delta^{18}\text{O}$  responses during late Pleistocene terminations, *Paleoceanography*, 24, PA3210, doi:10.1029/2009PA001732.
- Liu, Z., et al. (2008), CALIPSO lidar observations of the optical properties of Saharan dust: A case study of long-range transport, *J. Geophys. Res.*, 113, D07207, doi:10.1029/2007JD008878.
- Locamini, R. A., A. V. Mishonov, J. I. Antonov, T. P. Boyer, H. E. Garcia, O. K. Baranova, M. M. Zweng, and D. R. Johnson (2010), *World Ocean Atlas 2009, Volume 1: Temperature*, NOAA Atlas NESDIS 68, edited by S. Levitus, 184 pp., U.S. Government Printing Office, Washington, D. C.
- Loubere, P., and M. Richaud (2007), Some reconciliation of glacial-interglacial calcite flux reconstructions for the eastern equatorial Pacific, *Geochem. Geophys. Geosyst.*, 8, Q03008, doi:10.1029/2006GC001367.
- Loubere, P., F. Mekik, R. Francois, and S. Pichat (2004), Export fluxes of calcite in the eastern equatorial Pacific from the last glacial maximum to the present, *Paleoceanography*, 19, PA2018, doi:10.1029/2003PA000986.
- Lyle, M., D. M. Murray, B. P. Finney, J. Dymond, J. M. Robbins, and K. Brooksforce (1988), The record of Late Pleistocene biogenic sedimentation in the eastern tropical Pacific Ocean, *Paleoceanography*, 3(1), 39–59.
- Lyle, M., A. Mix, and N. Pisias (2002), Patterns of  $\text{CaCO}_3$  deposition in the eastern tropical Pacific Ocean for the last 150 kyr: Evidence for a southeast Pacific depositional spike during marine isotope stage (MIS) 2, *Paleoceanography*, 17(2), 1013, doi:10.1029/2000PA000538.
- Lyle, M., N. Mitchell, N. Pisias, A. Mix, J. I. Martinez, and A. Paytan (2005), Do geochemical estimates of sediment focusing pass the sediment test in the equatorial Pacific, *Paleoceanography*, 20, PA1005, doi:10.1029/2004PA001019.
- Lyle, M., N. Pisias, A. Paytan, J. I. Martinez, and A. Mix (2007), Reply to comment by R. Francois et al. on “Do geochemical estimates of sediment focusing pass the sediment test in the equatorial Pacific?”: Further explorations of Th-230 normalization, *Paleoceanography*, 22, PA1217, doi:10.1029/2006PA001373.
- Mahowald, N. M. (2007), Anthropocene changes in desert area: Sensitivity to climate model predictions, *Geophys. Res. Lett.*, 34, L18817, doi:10.1029/2007GL030472.
- Mahowald, N. M., D. R. Muhs, S. Levis, P. J. Rasch, M. Yoshioka, C. S. Zender, and C. Luo (2006), Change in atmospheric mineral aerosols in response to climate: Last glacial period, preindustrial, modern, and doubled carbon dioxide climates, *J. Geophys. Res.*, 111, D10202, doi:10.1029/2005JD006653.
- Marcantonio, F., R. F. Anderson, S. Higgins, M. Stute, P. Schlosser, and P. Kubik (2001), Sediment focusing in the central equatorial Pacific Ocean, *Paleoceanography*, 16(3), 260–267.
- Marchal, O., R. Francois, and F. Joos (2000), Ocean thermohaline circulation and sedimentary  $^{231}\text{Pa}/^{230}\text{Th}$  ratio, *Paleoceanography*, 15(6), 625.
- Martin, P. A., D. W. Lea, Y. Rosenthal, N. J. Shackleton, M. Samthein, and T. Papenfuss (2002), Quaternary deep sea temperatures derived from benthic foraminiferal Mg/Ca, *Earth Planet. Sci. Lett.*, 198, 193–209.
- Martinez, P., and R. S. Robinson (2010), Increase in water column denitrification during the last deglaciation: The influence of oxygen demand in the eastern tropical Pacific, *Biogeosciences*, 7, 1–9, doi:10.1029/2008PA001702.
- McCave, I. N., and I. R. Hall (2006), Size sorting in marine muds: Processes, pitfalls and prospects for paleoflow-speed proxies, *Geochem. Geophys. Geosyst.*, 7, Q10N05, doi:10.1029/2006GC001284.
- McGee, D., F. Marcantonio, and J. Lynch-Stieglitz (2007), Deglacial changes in dust flux in the eastern equatorial Pacific, *Earth Planet. Sci. Lett.*, 257, 215–230.
- McGee, D., F. Marcantonio, J. F. McManus, and G. Winckler (2010), The response of excess  $^{230}\text{Th}$  and extraterrestrial  $^3\text{He}$  to sediment redistribution at the Blake Ridge, western North Atlantic, *Earth Planet. Sci. Lett.*, 299, 138–149.
- Menviel, L., A. Timmermann, A. Mouchet, and O. Timm (2008), Meridional reorganization of marine and terrestrial productivity during Heinrich events, *Paleoceanography*, 23, PA1203, doi:10.1029/2007PA001445.
- Merkel, U., M. Prange, and M. Schulz (2010), ENSO variability and teleconnections during glacial times, *Quat. Sci. Rev.*, 29, 86–100, doi:10.1016/j.quascirev.2009.11.006.
- Mitchell, N. C., and J. M. Huthnance (2013), Geomorphological and geochemical evidence ( $^{230}\text{Th}$  anomalies) for cross-equatorial currents in the central Pacific, *Deep Sea Res., Part I*, 78(0), 24–41, doi:10.1016/j.dsr.2013.04.003.
- Mitchell, T. P., and J. M. Wallace (1992), The annual cycle of equatorial convection and sea surface temperature, *J. Clim.*, 5, 1140–1156.
- Multiza, S., M. Prange, J.-B. Stuut, M. Zabel, T. von Döbenek, A. C. Itambi, J. Nizou, M. Schulz, and G. Wefer (2008), Sahel megadroughts triggered by glacial slowdowns of Atlantic meridional overturning, *Paleoceanography*, 23, PA4206, doi:10.1029/2008PA001637.
- Pahnke, K., J. P. Sachs, L. Keigwin, A. Timmermann, and S.-P. Xie (2007), Eastern tropical Pacific hydrologic changes during the past 27,000 years from D/H ratios in alkenones, *Paleoceanography*, 22, PA4214, doi:10.1029/2007PA001468.
- Paytan, A., M. Lyle, A. Mix, and Z. Chase (2004), Climatically driven changes in oceanic processes throughout the equatorial Pacific, *Paleoceanography*, 19, PA4017, doi:10.1029/2004PA001024.
- Pena, L., I. Cacho, P. Ferretti, and M. A. Hall (2008), El-Niño-Southern Oscillation-like variability during glacial terminations and interlatitudinal teleconnections, *Paleoceanography*, 23, PA3101, doi:10.1029/2008PA001620.
- Prahl, F., L. Muehlhausen, and D. Zahnle (1988), Further evaluation of long-chain alkenones as an indicator of paleoceanographic conditions, *Geochim. Cosmochim. Acta*, 52, 2303–2310.
- Prospero, J. M., and E. Bonatti (1969), Continental dust in the atmosphere of the eastern equatorial Pacific, *J. Geophys. Res.*, 74(13), 3362–3371.
- Prospero, J. M., and P. J. Lamb (2003), African droughts and dust transport to the Caribbean: Climate change implications, *Science*, 302(5647), 1024–1027, doi:10.1126/science.1089915.
- Prospero, J. M., E. Bonatti, C. Schubert, and T. N. Carlson (1970), Dust in Caribbean atmosphere traced to African dust storm, *Earth Planet. Sci. Lett.*, 9(3), 287–293, doi:10.1016/0012-821x(70)90039-7.
- Rea, D. K. (1994), The paleoclimatic record provided by eolian deposition in the deep sea: The geologic history of wind, *Rev. Geophys.*, 32(2), 159–195.
- Rein, B., A. Luckge, L. Reinhardt, F. Sirocko, A. Wolf, and W. C. Dullo (2005), El Niño variability off Peru during the last 20,000 years, *Paleoceanography*, 20, PA4003, doi:10.1029/2004PA001099.
- Robinson, R. S., P. Martinez, L. D. Pena, and I. Cacho (2009), Nitrogen isotopic evidence for deglacial changes in nutrient supply in the eastern equatorial Pacific, *Paleoceanography*, 24, PA4213, doi:10.1029/2008PA001702.
- Sakai, K., and R. Kawamura (2009), Remote response of the East Asian winter monsoon to tropical forcing related to El Niño-Southern Oscillation, *J. Geophys. Res.*, 114, D06105, doi:10.1029/2008JD010824.
- Saukel, C., F. Lamy, J.-B. W. Stuut, R. Tiedemann, and C. Vogt (2011), Distribution and provenance of wind-blown SE Pacific surface sediments, *Mar. Geol.*, 280, 130–142.
- Schneider, B., G. Leduc, and W. Park (2010), Disentangling seasonal signals in Holocene climate trends by satellite-model-proxy integration, *Paleoceanography*, 25, PA4217, doi:10.1029/2009PA001893.
- Schneider, D. P., Y. Okumura, and C. Deser (2012), Observed Antarctic interannual climate variability and tropical linkages, *J. Clim.*, 25(12), 4048–4066, doi:10.1175/jcli-d-11-00273.1.
- Scholten, J. C., et al. (2005), Radionuclide fluxes in the Arabian Sea: The role of particle composition, *Earth Planet. Sci. Lett.*, 230(3–4), 319–337.
- Shackleton, N. J. (2000), The 100,000-year ice-age cycle identified and found to lag temperature, carbon dioxide, and orbital eccentricity, *Science*, 289, 1897–1902.
- Shackleton, N. J., and N. G. Pisias (1985), Atmospheric carbon dioxide, orbital forcing, and climate, in *The Carbon Cycle and Atmospheric CO<sub>2</sub>: Natural Variations Archean to Present*, edited by E. Sundquist and W. S. Broecker, pp. 303–317, AGU, Washington, D. C.
- Siddall, M., R. F. Anderson, G. Winckler, G. M. Henderson, L. I. Bradtmiller, D. McGee, A. Franzese, T. F. Stocker, and S. A. Mueller (2008), Modeling the particle flux effect on distribution of  $^{230}\text{Th}$  in the equatorial Pacific, *Paleoceanography*, 23, PA2208, doi:10.1029/2007PA001556.
- Singh, A. K., F. Marcantonio, and M. Lyle (2011), Sediment focusing in the Panama Basin eastern equatorial Pacific, *Earth Planet. Sci. Lett.*, 309, 33–44.
- Singh, A. K., F. Marcantonio, and M. Lyle (2013), Water column  $^{230}\text{Th}$  systematics in the eastern equatorial Pacific Ocean and implications for sediment focusing, *Earth Planet. Sci. Lett.*, 362, 294–304, doi:10.1016/j.epsl.2012.12.006.
- Skinner, L. C., and N. J. Shackleton (2005), An Atlantic lead over Pacific deep-water change across Termination I: Implications for the application of the marine isotope stage stratigraphy, *Quat. Sci. Rev.*, 24, 571–580.
- Spero, H. J., and D. W. Lea (2002), The cause of carbon isotope minimum events at glacial terminations, *Science*, 296, 522–525.
- Stehr, J. W., W. P. Ball, R. R. Dickerson, B. G. Doddridge, C. A. Piety, and J. E. Johnson (2002), Latitudinal gradients in O<sub>3</sub> and CO during INDOEX 1999, *J. Geophys. Res.*, 107(D19), 8016, doi:10.1029/2001JD000446.
- Stocker, T. F., A. Timmermann, M. Renold, and O. Timm (2007), Effects of salt compensation on the climate model response in simulations of large changes of the Atlantic meridional overturning circulation, *J. Clim.*, 20(24), 5912–5928, doi:10.1175/2007jcli1662.1.

- Takahashi, T., et al. (2009), Climatological mean and decadal change in surface ocean pCO<sub>2</sub>, and net sea-air CO<sub>2</sub> flux over the global oceans, *Deep Sea Res., Part II*, 56(8–10), 554–577, doi:10.1016/j.dsr2.2008.12.009.
- Taylor, S. R., and S. M. McClelland (1985), *The Continental Crust: Its Composition and Evolution*, pp. 312, Blackwell Scientific Publications, Oxford, London, Edinburgh, Boston, Palo Alto, Melbourne.
- Tesdal, J. E., E. D. Galbraith, and M. Kienast (2013), Nitrogen isotopes in bulk marine sediment: Linking seafloor observations with subseafloor records, *Biogeosciences*, 10(1), 101–118, doi:10.5194/bg-10-101-2013.
- Timmermann, A., S. J. Lorenz, S. I. An, A. Clement, and S. P. Xie (2007a), The effect of orbital forcing on the mean climate and variability of the tropical Pacific, *J. Clim.*, 20(16), 4147–4159, doi:10.1175/jcli4240.1.
- Timmermann, A., et al. (2007b), The influence of a weakening of the Atlantic meridional overturning circulation on ENSO, *J. Clim.*, 20(19), 4899–4919, doi:10.1175/jcli4283.1.
- Wang, C., and D. B. Enfield (2001), The tropical Western Hemisphere warm pool, *Geophys. Res. Lett.*, 28(8), 1635–1638.
- Wang, C., S. Dong, A. T. Evan, G. R. Foltz, and S.-K. Lee (2012), Multidecadal covariability of North Atlantic sea surface temperature, African dust, Sahel rainfall, and Atlantic hurricanes, *J. Clim.*, 25, 5404–5415.
- Winckler, G., R. F. Anderson, M. Q. Fleischer, D. McGee, and N. Mahowald (2008), Covariant Glacial-Interglacial dust fluxes in the Equatorial Pacific and Antarctica, *Science*, 320, 93–96.
- Xie, S.-P. (1994), On the genesis of the equatorial annual cycle, *J. Clim.*, 7.
- Xie, R. C., and F. Marcantonio (2012), Deglacial dust provenance changes in the eastern equatorial Pacific and implications for ITCZ movement, *Earth Planet. Sci. Lett.*, 317–318, 386–395.
- Xie, S.-P., Y. Okumura, T. Miyama, and A. Timmermann (2008), Influences of Atlantic climate change on the tropical Pacific via the Central American Isthmus, *J. Clim.*, 21(15), 3914–3928, doi:10.1175/2008jcli2231.1.
- Yu, E.-F., R. Francois, M. P. Bacon, and A. P. Fleer (2001), Fluxes of <sup>230</sup>Th and <sup>231</sup>Pa to the deep sea: Implications for the interpretation of excess <sup>230</sup>Th and <sup>231</sup>Pa/<sup>230</sup>Th profiles in sediments, *Earth Planet. Sci. Lett.*, 191, 219–230.
- Zhang, R., and T. L. Delworth (2005), Simulated tropical response to a substantial weakening of the Atlantic thermohaline circulation, *J. Clim.*, 18, 1853–1860.